NUMERICAL SIMULATION OF DYNAMIC MECHANICAL PROPERTIES OF GRAPHENE-REINFORCED ALUMINUM MATRIX COMPOSITES

NUMERIČNA SIMULACIJA DINAMIČNIH MEHANSKIH LASTNOSTI KOMPOZITOV Z MATRICO NA OSNOVI ALUMINIJA, OJAČANO Z GRAFENOM

Xiaoming Du*, Zhixuan Lu, Shuang Guo

School of Materials Science and Engineering, Shenyang Ligong University, Shenyang, China

The effects of the strain rate of dynamic loading, volume fraction, shapes and orientation of graphene on the dynamic mechanical properties, deformation and damage of graphene/7075Al composites were simulated using the finite element method, and the damage mechanism of the composites under dynamic load was revealed. The flow strain-stress curves were obtained. The effect of strain rates on the flow stress of the composites was analyzed. The results show that graphene/7075Al composites exhibit a significant strain rate effect. With an increase in the volume fraction of graphene, the yield strength of the composites increases and the composites have significant stress-softening characteristics at a strain rate of 10000 s^{-1}, leading to a reduced strain-hardening effect. The shape and orientation of graphene have an important influence on the dynamic mechanical properties and the extent of damage made to the composites. The flow stress of the composites increases with varying the graphene shape and orientation in the following order, respectively: prism < cylinder < platelet < disc and $0° < 3D < 90° < 45°$. The extent of the damage to the composites increases in the following order: disc < platelet < cylinder < prism and $0° < 3D < 90° < 45°$. The dynamic failure mechanism of graphene/7075Al composites is interface damage.

Keywords: aluminum matrix composites, graphene, dynamic mechanical properties, numerical simulation

Avtorji v članku opisujejo vpliv hitrosti deformacije med dinamičnim obremenjevanjem, volumskega deleža, oblike in orientacije grafena na dinamične mehanske lastnosti, deformacijo in poškodbe nastale na kompozitu vrste grafen/Al7075. Simulacije so izvajali s pomočjo metode končnih elementov in mehanizma poškodb na izbranem kompozitu pod pogoji dinamičnih obremenitev. Določili so prave krivulje tečenja napetost-deformacija. Analizirali so občutljivost krivulj tečenja kompozita na hitrost deformacije. Rezultati analiz so pokazali, da ima hitrost deformacije zelo velik vpliv na izbrani kompozit grafen/Al7075. Z naraščanjem volumskega deleža grafena je naraščala meja tečenja kompozita in nastopilo je pomembno napetostno mehčanje kompozita pri hitrosti deformacije 10000 s^{-1}. S tem je bil zmanjšan učinek deformacijskega utrjevanja. Oblika in orientacija grafena sta pomembno vplivala na dinamične mehanske lastnosti in nastanek oz. širjenje poškodb izbranega kompozita. Napetost tečenja kompozita je naraščala s spreminjanjem oblike in orientacije grafena v naslednjem vrstnem redu: prizme < valjčki < ploščice < diski in $0° < 3D < 90° < 45°$. Povečevanje širjenja poškodb je potekalo v naslednjem vrstnem redu: disk < ploščice < valjčki < prizme in $0° < 3D < 90° < 45°$. Mehanizem nastanka dinamičnih poškodb izbranega kompozita vrste grafen/Al7075 je potekal na mejah kovinska matrica-grafen.

Ključne besede: kompoziti s kovinsko matrico, aluminij, grafen, dinamične mehanske lastnosti, numerična simulacija

1 INTRODUCTION

Aluminium matrix composites (AMCs) are widely used in the aerospace, automotive and marine industry, electronic packaging and other fields because of their excellent comprehensive properties, such as low density, high specific strength, high specific stiffness, wear and corrosion resistance, good thermal conductivity and so on.[1–5] To obtain a desired performance, a new generation of carbonaceous nanomaterials, graphene, was adopted for strengthening AMCs. The merits of graphene-reinforced aluminium matrix composites are their superior mechanical properties and excellent wear resistance. Moreover, an improvement in the electrical conductivity and thermal conductivity in comparison with an unreinforced alloy was also reported.[6–8]

The current studies of graphene-reinforced aluminium matrix composites still focus on the static mechanical properties.[9–12] The equipment used in aerospace, armor protection and other fields will often be subjected to impact loads during service. However, there are few reports on the dynamic mechanical properties of graphene-reinforced aluminium matrix composites. Friend and Nixon studied the mechanical properties of aluminium matrix composites under impact load.[13] Tan et al. studied the dynamic mechanical properties of SiC-particle-reinforced 2024 aluminium alloy and found that the composite showed obvious strain rate sensitivity.[14] Yadav et al. studied the mechanical properties of 20 % Al_2O_3 particle-reinforced aluminium matrix composites under quasi-static compression, dynamic com-

*Corresponding author's e-mail:
du511@163.com (Xiaoming Du)

pression, torsion and high-speed impact.[15] It was found that when the strain rate exceeded 1000 s^{-1}, the composites showed obvious strain rate sensitivity effect compared with the matrix. Perng et al. found that the strain rate sensitivity of composites increased with an increase in the reinforcing phase content.[16]

In recent years, with the development of the finite element method (FEM), we can effectively simulate the dynamic impact compression of composites so as to better understand the dynamic compression mechanical behavior of materials. Fathipour et al. used the finite element method to establish a model to predict the failure strain of composites.[17] Prabu et al. established a micro finite element model of particle-reinforced aluminum matrix composites. They studied the failure mechanism of composites under tensile load.[18] Li et al. simulated the mechanical properties of particle-reinforced metal matrix composites under high strain rate using a single-cell finite element model, and studied the effects of different particle shapes, volume fractions and aspect ratios on the mechanical properties of composites.[19] Song et al. used the finite element analysis to study the mechanical properties and fracture behavior of graphene-reinforced aluminum matrix composites considering damage and failure behavior. The simulated results were in good agreement with the experimental results.[20]

In this paper, a finite element model based on the real microstructure of graphene-reinforced aluminum matrix composites was established. The dynamic mechanical properties of graphene/Al composites were numerically simulated using the finite element method. The effects of the strain rate, volume fraction, shape, orientation of graphene, strain hardening and strain rate hardening on the deformation and damage evolution of the composites under the condition of dynamic loading were analyzed.

2 EXPERIMENTAL PART

2.1 Microstructural model

A three-dimensional model of a cubic unit cell was built using the DIGIMAT software, 10 mm in length. In the present work, graphene was assumed to have four shapes, namely, a disc approximately representing few-layer graphene, a platelet, a cylinder and a prism, the shapes of graphene with different degrees of agglomeration and stacking, as shown in **Figure 1**. The ratio of thickness to diameter was in a range of 0.01–0.1 for different graphene shapes. We considered the volume fraction of the reinforcement to be (1, 2, 3, 4 and 6) φ/%. The interface between the reinforcement and the matrix was assumed to have perfect adherence. The orientation angle of graphene sheets was defined by the angle between the graphene sheets and the X-axis. Models with 0°, 45°, 90° and random orientation (3D) were established.

2.2 Material model

The 7075Al alloy was selected as the matrix material and flake graphene was the reinforcing phase. The constitutive equation of a material describes the relationship between the rheological stress of the material and the parameters, such as strain, strain rate and homologous temperature during deforming. The following Johnson-Cook (J-C) constitutive equation was used for the aluminum matrix composites in this study:[21]

$$\sigma = (A + B\varepsilon^n)(1 + C \ln \dot{\varepsilon}^*)(1 - T^{*m}) \qquad (1)$$

$$\dot{\varepsilon}^* = \frac{\dot{\varepsilon}}{\dot{\varepsilon}_0} \qquad (2)$$

$$T^* = \frac{(T - T_r)}{(T_m - T_r)} \qquad (3)$$

Here, A, B, C and m are material constants and n is the strain hardening index; σ is the flow stress; ε, $\dot{\varepsilon}$ and $\dot{\varepsilon}_0$ are the plastic strain, strain rate and reference strain rate, respectively; $\dot{\varepsilon}^*$ and T^* are the non-dimensional variables defined in Equations (2) and (3); T, T_r and T_m are the test temperature, reference temperature and melting point temperature of the material, respectively.

All the tests in this work were carried out at room temperature, regardless of the temperature softening effect of the material. Equation (1) was simplified as Equation (4):

$$\sigma = (A + B\varepsilon^n)(1 + C \ln \dot{\varepsilon}^*) \qquad (4)$$

Graphene was assumed to be a linear elastic material following generalized Hooke's law. Graphene fracture omitted for simplicity and graphene debonding occurred
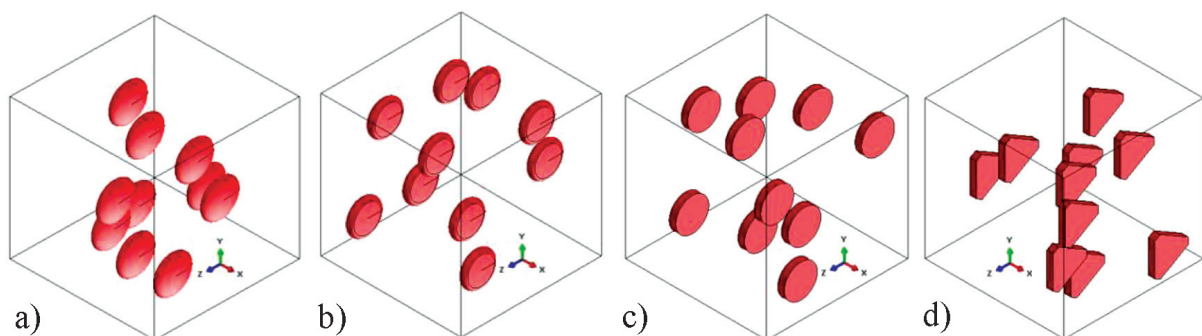

Figure 1: Graphene/7075Al composite models with different graphene shapes for 90° orientation angle: a) disc, b) platelet, c) cylinder, d) prism
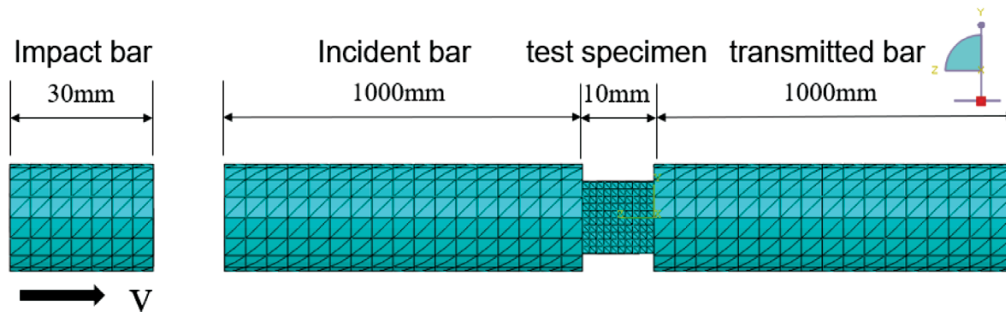
Figure 2: Diagram of the SHPB model including boundary conditions and loading mode

due to the matrix failure around it. Graphene has a density of 2.267 g/cm, an elastic modulus of 1086 GPa and a Poisson's ratio of 0.17.[22–24] The material properties of 7075Al are given in **Table 1**.

Table 1: Material properties of 7075Al[25]

Density (g/cm)	Elastic modulus (GPa)	Poisson's ratio	A (MPa)	B (MPa)	C	n
2.8	71	0.3	473	210	0.033	0.3813

2.3 Finite element model and boundary conditions

The simulation of dynamic mechanical properties was based on a split-Hopkinson pressure bar (SHPB). By establishing a SHPB experimental device model, the dynamic mechanical properties of aluminum matrix composites were calculated. However, the structure of the SHPB device system used in the experiment was complex, including multiple components. If all of them had been used in the simulation process, the model would have been very complex. The amount of calculations would have been very large. Therefore, in order to facilitate the modeling and simplify the amount of calculations, the SHPB device was simplified, but it was also ensured that the simulation results were not distorted. **Figure 2** shows the boundary-condition setting and the loading mode of the SHPB experimental system model. The loading was to provide specific impact velocity to the bullet model, and the corresponding strain rate was obtained by setting different impact velocities.

A finite element analysis was performed using a commercial software package (ABAQUS 6.14). The analysis was conducted under a three-dimensional stress. Modified quadratic tetrahedron elements were used for both the metal matrix and graphene particles. Totally, the models contained about 53000 elements. The verification function in the software was used to check and correct the distorted mesh to allow the calculation. The mesh size was iteratively refined to minimize stress singularities and achieve convergence. The mesh refinement was conducted until the overall stress–strain curve output from a model was unchanged. The matrix and graphene adopted perfect interface bonding and a surface-to-surface contact. The analysis was conducted under plane

strain. The right edge of a composite model was fixed in the X-direction, and the load was applied to the left edge of the model by the bullet along the X-axis (**Figure 2**), making the load propagate between the elements in the form of a stress wave. When the calculation was completed, a subroutine was used to extract the stress-strain relationship of the model for the next analysis.

3 RESULTS AND DISCUSSION

3.1 Strain rate effect

Figure 3 shows the flow stress-strain curves obtained with the simulation for the 7075Al alloy and graphene/7075Al composite with a volume fraction of 2 % of graphene at room temperature and at different strain rates. The graphene shape is platelet with an orientation of 90°. It was found that the flow stress increased nonlinearly with the increase in the flow strain. This phenomenon is called strain hardening, indicating that the material enters the plastic deformation stage. As can be seen from **Figure 3a**, when the strain rate of the 7075Al alloy is 1000 s⁻¹ and 2000 s⁻¹, the flow stress-strain curves are almost identical , indicating that the flow stress of the 7075Al alloy is not sensitive to the strain rate under this condition. As the strain rate increases to 5000 s⁻¹ and 8000 s⁻¹, the flow stress of the alloy increases obviously. When the strain rate increases to 10000 s⁻¹, the flow stress of the alloy shows no obvious change compared with 8000 s⁻¹.

The flow stress of the graphene/7075Al composite increases with the increase in the strain rate, as shown in **Figure 3b**. When the strain rate is between 1000 s⁻¹ and 5000 s⁻¹, the flow stress increases slightly, while the flow stress of the composite increases greatly with the strain rate from 8000 s⁻¹ to 10000 s⁻¹, showing an obvious strain rate reinforcing effect. In addition, it can be also found that the graphene/7075Al composite shows the stress softening characteristic above the 20 % strain at a strain rate of 10000 s⁻¹.

3.2 Graphene volume fraction effect

The dynamic compression simulations of graphene/7075Al composites with different graphene volume fractions were conducted at a strain rate of 10000 s⁻¹, in
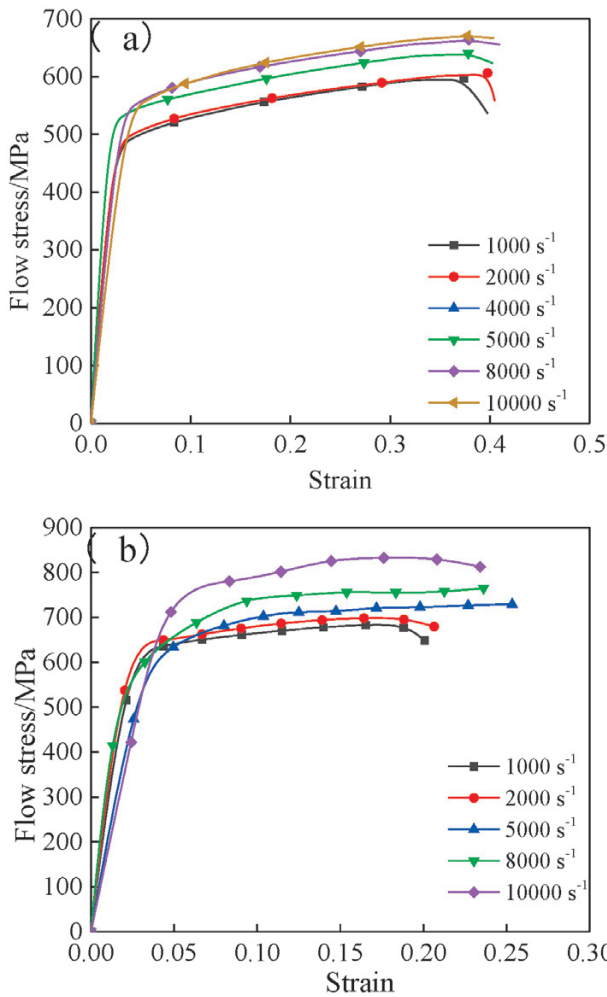
Figure 3: Flow stress-strain curves of the materials at different strain rates: a) 7075Al, b) 2 φ/% graphene/7075Al

which the graphene shape was a platelet and the orientation was 0°. The flow stress-strain curves are shown in
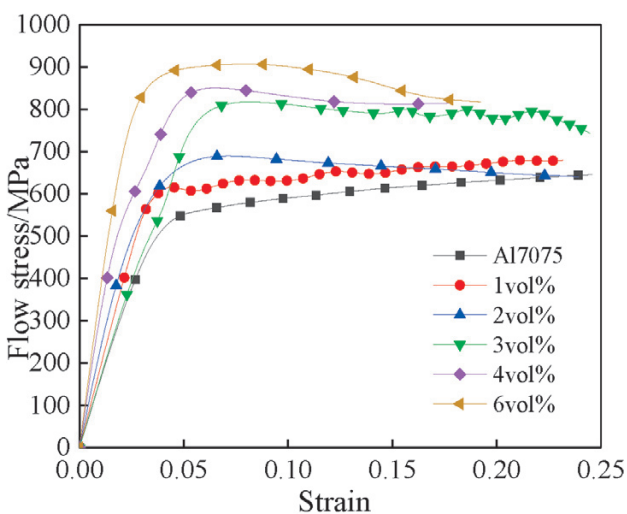

Figure 4: Flow stress-strain curves of graphene/7075Al composites with different graphene volume fractions

Figure 4. It can be clearly seen that the flow stress of the composite increases with the increase in the graphene volume fraction, showing an obvious enhancement effect. The reason for this is the fact that the higher the graphene volume fraction, the higher are the grain refinement and dislocation interactions in the matrix, resulting in a higher level of the flow stress in the composites. According to the Orowan dislocation theory, the curvature radius of dislocations also increases with the increasing reinforcement volume fraction, leading to a higher flow stress.

When the compression strain exceeded 5 % at the strain rate of 10000 s^{-1} for the composites with the graphene volume fraction higher than 2 %, the flow stress decreased and the stress softening characteristic was present. There was an obvious inflexion point near the 5 % strain, after which the value of the flow stress descended. The reason for this was the fact that the deformation of the material during the SHPB tests could be considered as an adiabatic condition and in that course the heat resulting from plastic deformation was too late to be dispersed, which led to the formation of a local thermal stress area and the heat was accumulated so that the matrix was softened and the value of the flow stress decreased.[26] Under dynamic load, the graphene sheets hardly showed any plastic deformation, so the plastic deformation of the whole material was produced by the aluminum matrix. A large local plastic strain and a strain rate were produced in the aluminum matrix, and a large amount of heat was produced. This led to aluminum matrix softening, reducing the strain hardening effect. With the increase in the graphene volume fraction, the response of the composites to the load, including matrix deformation and load transfer, was gradually transferred to the graphene sheets that bore the load by forming a network structure. This intensified the damage of the interface between the graphene and aluminum matrix, making the composites prone to adiabatic shear failure.

3.3 Graphene shape effect

The dynamic compression simulations of the graphene/7075Al composites containing different graphene shapes were performed at strain rates of 1000 s^{-1} and 10000 s^{-1} where the graphene volume fraction was 3 % and the graphene orientation was 90°. The flow stress-strain curves are shown in **Figure 5**. It was found that the disc-shaped graphene exhibited a more significant strengthening effect than those of the other three shapes at strain rates of 1000 s^{-1} and 10000 s^{-1}. This is because the disc-shaped graphene was similar to the few-layer graphene, creating a more effective interface and better bonding between the matrix and the reinforcement. When the composites deformed, the matrix deformation between the layers of graphene allowed a high incidence of dislocation formation. Stress concentrations at the dislocation accumulated, wherein the dislocation movement was obstructed in graphene by a high

specific surface area. During the deformation, the flow stress increased since moving dislocations were blocked by graphene. The lower the number of graphene layers, the higher was the number of graphene sheets, and the stronger was the obstacle to the dislocation movement. Moreover, it is considered that there are large numbers of edges and corners in cylindrical and prismatic graphene, making it easier for the material to cut the matrix, resulting in damaged interfaces between the graphene and aluminum matrix.

3.4 Graphene orientation effect

Figure 6 shows the flow stress-strain curves of the graphene/7075Al composites with different graphene orientations at strain rates of 1000 s^{-1} and 10000 s^{-1} where the graphene volume fraction was 2 % and graphene was disc-shaped. For a low strain rate (**Figure 6a**), it was found that the flow stress of the composites with a graphene orientation of 45° was the highest, followed by 90°. The flow stress of the composites with an orientation of 0° and random distribution (3D) was commensurate. For a high strain rate (**Figure 6b**), the
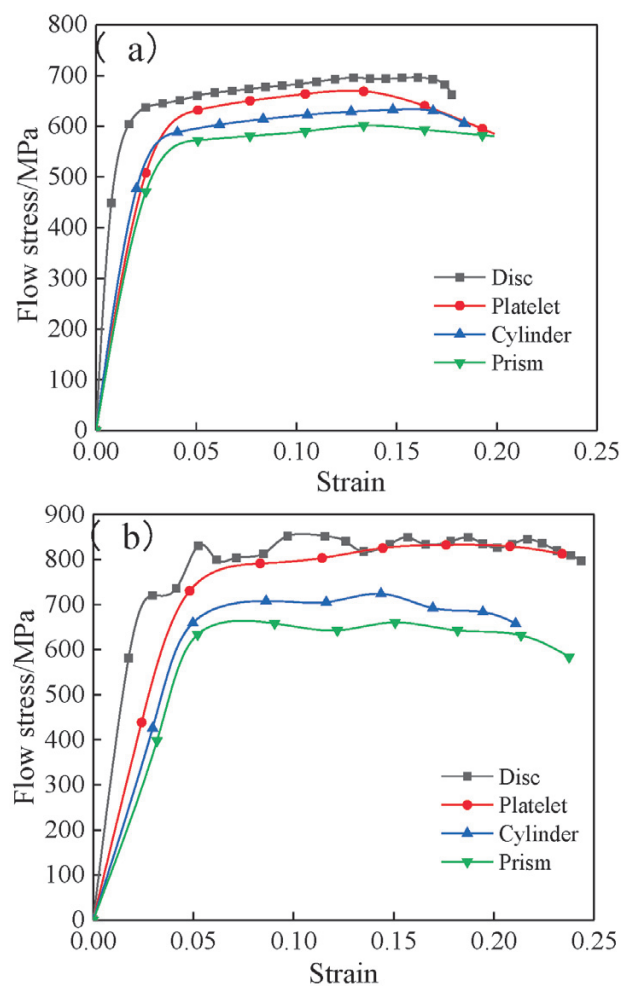

Figure 5: Flow stress-strain curves of graphene/7075Al composites with different graphene shapes: a) 1000 s^{-1}, b) 10000 s^{-1}
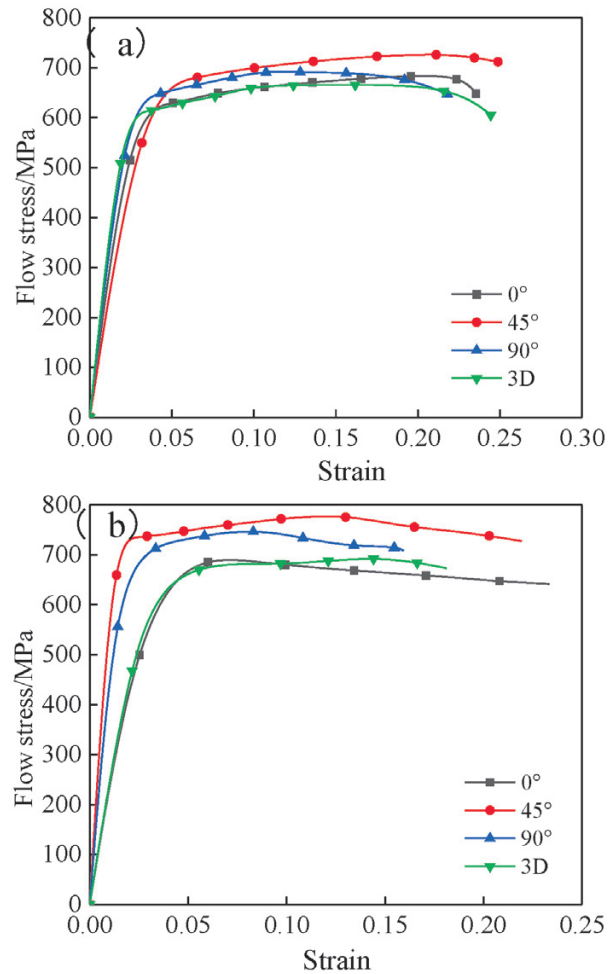

Figure 6: Flow stress-strain curves of graphene/7075Al composites with different graphene orientations: a) 1000 s^{-1}, b) 10000 s^{-1}

flow stress of the composites with graphene orientations of 45° and 90° was much greater than for 0° and random distribution (3D), indicating that the two oriented graphene-aluminum matrix composites showed a significant strain rate enhancement effect.

3.5 Dynamic damage mechanism

The failure mechanisms of high volume fraction particle reinforced aluminum matrix composites under a high strain rate mainly include particle fragmentation, local thermal softening of aluminum alloy and local adiabatic shear failure. However, there are few studies on the failure mechanism of graphene-reinforced aluminum matrix composites with a low volume fraction. In addition, due to a short loading time of the high strain rate and a lack of a real-time analysis of the conventional experimental methods, it is difficult to capture the information about the stress distribution, stress state and damage evolution in time. Therefore, it is necessary to study the deformation and damage evolution in composite materials during dynamic compression with the help of the numerical simulation method.

Figures 7 to **9** show the effects of the strain rate, graphene shape, graphene orientation on the stress distribution, deformation and damage evolution in graphene/7075Al composites under the impact compression load. It was found that under the impact load, the load was transferred from the matrix to graphene. Graphene exhibited high strength and no deformation, causing a high local stress concentration around graphene. Once the local stress is larger than the yield or fracture stress of the aluminum matrix, deformation and damage occur in the aluminum matrix. The damage of the composites depends upon the influence of the strain rate, graphene shape and graphene orientation.

Figure 7 shows the deformation and damage simulation results for the graphene/7075Al composite under different strain rates. The graphene volume fraction was 2 %. Graphene was in the shape of a disc. The orientation of graphene was 90°. It was found that with the increase in the strain rate, the deformation and damage of the composite became more and more serious. When the strain rate was 2000 s^{-1}, obvious stress concentration occurred around graphene. However, the stress concentration in the matrix near the graphene/7075Al interface was not obvious. It was mainly uniform plastic deformation (**Figure 7a**).
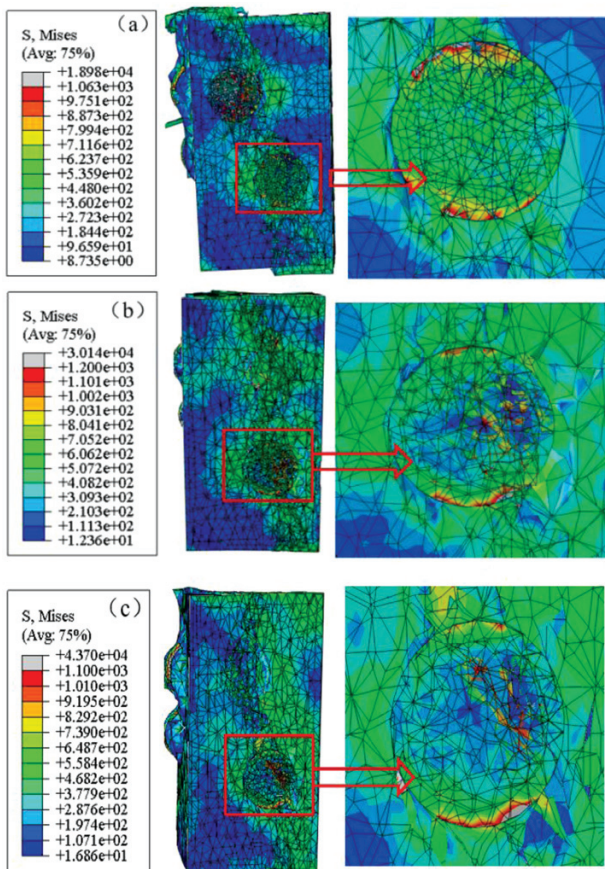
When the strain rate was 8000 s^{-1} and 10000 s^{-1}, a high stress concentration was present around the graphene. The stress in the matrix near the graphene/7075Al matrix interface exceeded 600 MPa, and the local stress in certain regions of the interface exceeded 750 MPa, as shown in **Figures 7b** and **7c**. The deformation of the matrix could not bear a large amount of stress concentration, resulting in the cracking of the interface between the matrix and graphene. A local grid failure occurred and then extended to the whole model. The failure mechanism is interface damage.

Figure 8 shows the deformation and damage simulation results for the graphene/7075Al composites with different graphene shapes at the strain rate of 10000 s^{-1}. The graphene volume fraction was 2 %. The orientation of
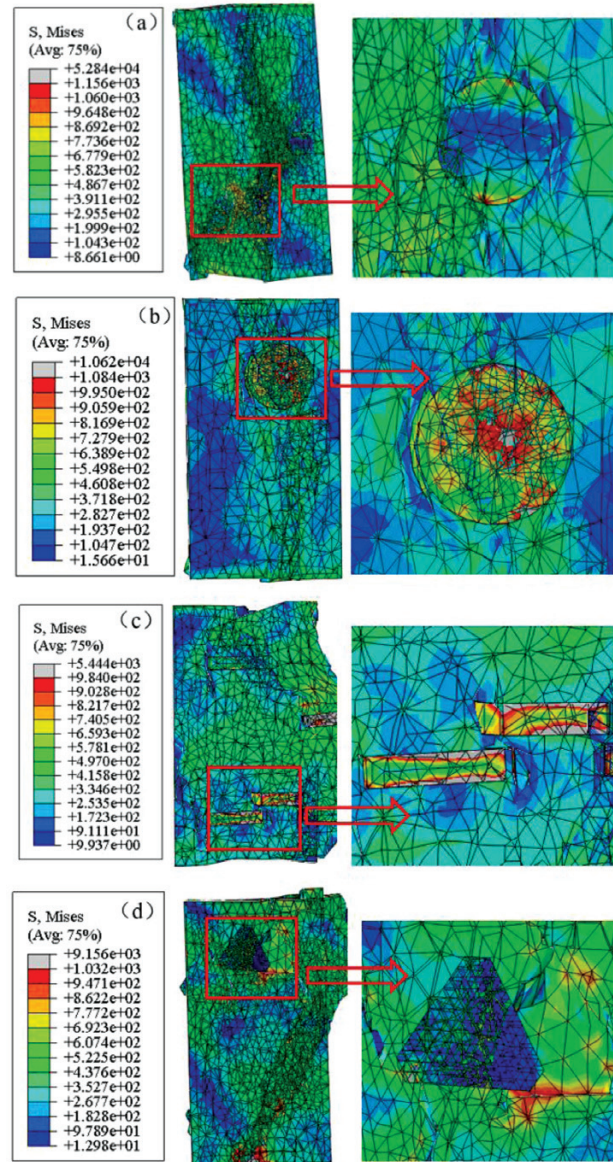

Figure 8: Distribution of the stress of graphene/7075Al composites with different graphene shapes at a strain rate of 10000 s^{-1}: a) disc, b) platelet, c) cylinder, d) prism

Figure 7: Distribution of the stress of graphene/7075Al composites at different strain rates: a) 2000 s^{-1}, b) 8000 s^{-1}, c) 10000 s^{-1}

graphene was 90°. On **Figure 8a**, we can see that when graphene was in the shape of a disc, the stress concentration around graphene was gentle, and the stress distribution in the matrix was relatively uniform. The stress concentration at the graphene/7075Al interface increased obviously, causing slight damage to one side of the matrix in the interface area. When graphene was in the shape of a platelet, the stress concentration around graphene was significantly enhanced, resulting in a stress concentration near the graphene/7075Al interface (**Figure 8b**). The meshes in the interface area were seriously deformed, aggravating the damage to the interface area. When graphene was shaped as a thin cylinder or a thin triangular prism, there was the most severe stress concentration in the matrix and interface area, as shown in **Figures 8c** and **8d**. The reason for this is the fact that the two graphene shapes with sharp edges and corners re-

sulted in a severe local stress concentration around graphene, causing damage to the matrix at the graphene/7075Al interface. This aggravated the damage to the composite. Therefore, the damage caused to the composites by different graphene shapes was in the order of disc < platelet < cylinder < prism. Here, too, the failure mechanism is interface damage.

Figure 9 shows the simulation results for the deformation and damage of the graphene/7075Al composites with different graphene orientations at a strain rate of 10000 s^{-1}. The graphene volume fraction was 2 %. Graphene was shaped as a disc. On **Figure 9a**, we can see that when the orientation of graphene was 0°, the local stress concentration was mainly around graphene, and the stress distribution in the matrix was relatively uniform. It was indicated that there was slight damage to the graphene/7075Al interface. This was because the orientation of graphene was parallel to the direction of impact loading where graphene had the least resistance to the dislocation movement during the stress transfer from the matrix to graphene. Moreover, the plastic deformation of the matrix was more uniform and the damage to the matrix and graphene/7075Al interface was slight. When the orientation of graphene was 45°, graphene initiated the strongest obstruction to the dislocation movement. This resulted in a severe stress concentration around graphene, as shown in **Figure 9b**. It was possible to aggravate the damage to the graphene/7075Al interface. The failure mechanism was interface damage. When the graphene orientation was 90°, the damage to the matrix in the interface region was the second largest damage (**Figure 9c**). When the orientation of graphene was randomly distributed (3D) (**Figure 9d**), the damage to the matrix in the interface region was much smaller. This was understandable as a random arrangement of graphene can better disperse the stress concentration caused by the impact load, reducing the stress concentration between the matrix and graphene to a certain extent. Therefore, the order of the damage to the composites caused by different graphene orientations was 0° < 3D < 90° < 45°.

Figure 9: Distribution of the stress of graphene/7075Al composites with different graphene orientations at a strain rate of 10000 s^{-1}: a) 0°, b) 45°, c) 90°, d) 3D

4 CONCUSIONS

Numerical simulations of the effects of the strain rate of dynamic loading, volume fraction, shapes and orientation of graphene on the dynamic mechanical properties, deformation and damage of graphene/7075Al composites were carried out. Simulation results show that graphene/7075Al composites exhibit an obvious strain-rate strengthening effect in the region of strain rates from 1000 s^{-1} to 10000 s^{-1}. With an increase in the volume fraction of graphene, the yield strength of the composites increases. When the volume fraction of graphene is more than 2 %, the composites exhibit significant stress-softening characteristics at a strain rate of 10000 s^{-1}, leading to a reduced strain-hardening effect. The shape and ori-
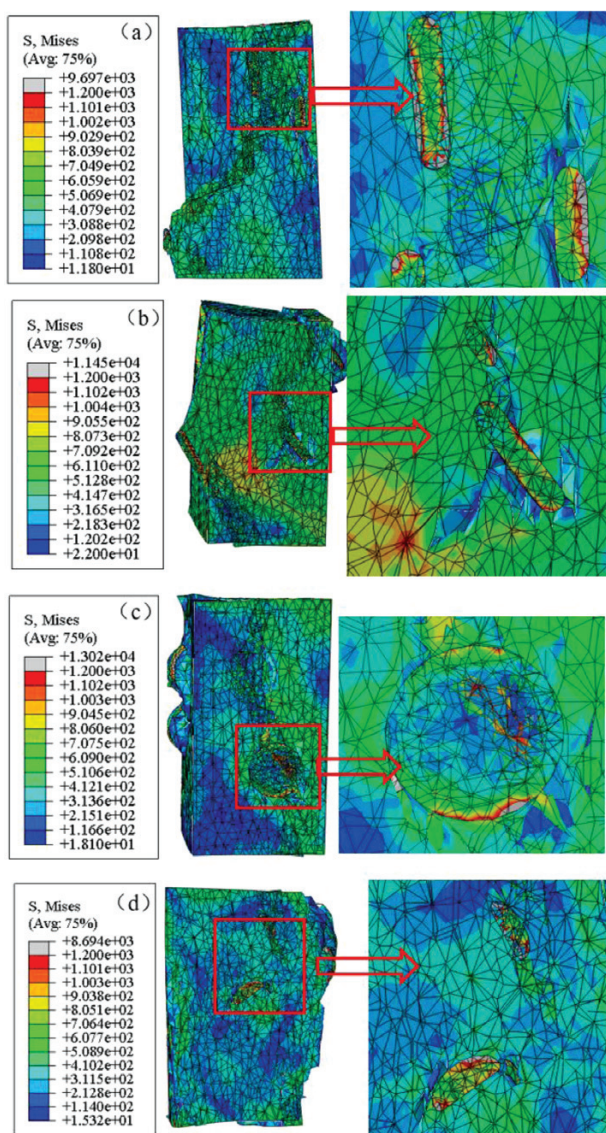
entation of graphene have an important influence on the dynamic mechanical properties and the extent of damage to the composites. The flow stress of the composites increases with varying graphene shape and orientation in the following order, respectively: prism < cylinder < platelet < disc and 0° < 3D < 90° < 45°. The extent of the damage to the composites increases in the following order: disc < platelet < cylinder < prism and 0° < 3D < 90° < 45°. The dynamic failure mechanism of graphene/7075Al composites is interface damage.

Acknowledgment

5 REFERENCES

[1] C. H. Jeon, Y. H. Jeong, J. J. Seo, H. N. Tien, S. T. Hong, Y. J. Yum, S. H. Hur, K. J. Lee, Material properties of graphene/aluminum metal matrix composites fabricated by friction stir processing, Int. J. Precis. Eng. Manuf., 15 (**2014**), 1235–1239, doi:10.1007/s12541-014-0462-2

[2] K. K. Alaneme, M. O. Bodunrin, Corrosion behavior of alumina reinforced aluminium (6063) metal matrix composites, Journal of Minerals & Materials Characterization & Engineering ,10 (**2011**) 12, 1153–1165, doi:10.4236/jmmce.2011.1012088

[3] V. Chak, H. Chattopadhyay, T. L. Dora, A review on fabrication methods, reinforcements and mechanical properties of aluminum matrix composites, Journal of Manufacturing Processes, 56 (**2020**), 1059–1074, doi:10.1016/j.jmapro.2020.05.042

[4] M. Kok, Production and mechanical properties of Al₂O₃ particle-reinforced 2024 aluminium alloy composites, Journal of Materials Processing Technology, 161 (**2005**) 3, 381–387, doi:10.1016/j.jmatprotec.2004.07.068

[5] N. S. Pourmand, H. Asgharzadeh, Aluminum Matrix Composites Reinforced with Graphene: A Review on Production, Microstructure, and Properties, Critical Reviews in Solid State and Materials Sciences, 45 (**2020**) 4, 1–49, doi:10.1080/10408436.2019.1632792

[6] W. Yang, Q. Zhao, L. Xin, J. Qiao, J. Zou, P. Shao, Z. Yu, Q. Zhang, G. Wu, Microstructure and mechanical properties of graphene nanoplates reinforced pure Al matrix composites prepared by pressure infiltration method, Journal of Alloys and Compounds, 732 (**2018**), 748–758, doi:10.1016/j.jallcom.2017.10.283

[7] M. Cao, Y. Luo, Y. Xie, Z. Tan, G. Fan, Q. Guo, Y. Su, Z. Li, D. B. Xiong, The influence of interface structure on the electrical conductivity of graphene embedded in aluminum matrix, Advanced Materials Interfaces, 6, (**2019**) 13, 1900468, doi:10.1002/admi.201900468

[8] A. Lu, L. Zhao, Y. Liu, Z. Li, D. B. Xiong, J. Zou, Q. Guo, Enhanced damping capacity in graphene–Al nanolaminated composite pillars under compression cyclic loading, Metallurgical and Materials Transactions A: Physical Metallurgy and Materials Science, 51 (**2020**) 4, 1463–1468, doi:10.1007/s11661-020-05632-4

[9] S. N. Alam, L. Kumar, Mechanical properties of aluminum based metal matrix composites reinforced with graphite nanoplatelets, Materials Science and Engineering A, 667 (**2016**), 16–32, doi:10.1016/j.msea.2016.04.054

[10] J. Li, Y. Xiong, X. Wang, S. Yan, C. Yang, W. He, J. Chen, S. Wang, X. Zhang, S. Dai, Microstructure and tensile properties of bulk nanostructured aluminum/graphene composites prepared via cryomilling, Materials Science and Engineering A, 626 (**2015**), 400–405, doi:10.1016/j.msea.2014.12.102

[11] S. Shin, H. Choi, J. Shin, D. Bae, Strengthening behavior of few-layered graphene/aluminum composites, Carbon, 82 (**2015**), 143–151, doi:10.1016/j.carbon.2014.10.044

[12] B. L. Dasari, M. Morshed, J. M. Nouri, D. Brabazon, S. Naher, Mechanical properties of graphene oxide reinforced aluminium matrix composites, Composites Part B: Engineering, 145 (**2018**), 136–144, doi:10.1016/j.compositesb.2018.03.022

[13] C. M. Friend, A. C. Nixon, Impact response of short ä-alumina fibre/aluminiumalloy metal matrix composites, Journal of Materials Science, 23 (**1988**) 6, 1967–1975, doi:10.1007/bf01115758

[14] Z. H.Tan, B. J. Pang, B. Z. Gai, G. H. Wu, B. Jia, The dynamic mechanical response of SiC particulate reinforced 2024 aluminum matrix composites, Materials Letters, 61 (**2007**) 23–24, 4606–4609, doi:10.1016/j.matlet.2007.02.069

[15] S. Yadav, D. R. Chichili, K. T. Ramesh, The mechanical response of a 6061-T6 Al/Al₂O₃ metal matrix composite at high rates of deformation, Acta Metallurgica et Materialia, 43 (**1995**) 12, 4453–4464, doi:10.1016/0956-7151(95)00123-d

[16] C. C. Perng, J. R. Hwang , J. L. Doong, High strain rate tensile properties of an (Al₂O₃ particles)-(Al alloy 6061-T6) metal matrix composite, Materials Science and Engineering A, 171 (**1993**) 1–2, 213–221, doi:10.1016/0921-5093(93)90408-7

[17] L. M. Tham, M. Gupta, L. Cheng, Predicting the failure strains of Al/SiC composites with reacted matrix–reinforcement interfaces, Materials Science & Engineering A, 354 (**2003**) 1, 369–376, doi:10.1016/S0921-5093(03)00040-6

[18] S. B. Prabu, L. Karunamoorthy, Microstructure-based finite element analysis of failure prediction in particle-reinforced metal–matrix composite, Journal of Materials Processing Tech., 207 (**2008**) 1–3, 53–62, doi:10.1016/j.jmatprotec.2007.12.077

[19] Y. Li, K. T. Ramesh, Influence of particle volume fraction, shape, and aspect ratio on the behavior of particle-reinforced metal-matrix composites at high rates of strain, Acta Materialia, 46 (**1998**) 16, 5633–5646, doi:10.1016/S1359-6454(98)00250-X

[20] Y. Song, Y. Ma, K. Zhan, Simulations of deformation and fracture of graphene reinforced aluminium matrix nanolaminated composites, Mechanics of Materials, 142 (**2019**), 103283–103283, doi:10.1016/j.mechmat.2019.103283

[21] Z. Jia, B. Guan, Y. Zang, Y. Wang, L. Mu, Modified Johnson-Cook model of aluminum alloy 6016-T6 sheets at low dynamic strain rates, Materials Science & Engineering A, 820 (**2021**), 141565, doi:10.1016/j.msea.2021.141565

[22] A. Nieto, A. Bisht, D. Lahiri, C. Zhang, A. Agarwal, Graphene reinforced metal and ceramic matrix composites: a review, Int. Mater. Rev., 62 (**2017**) 5, 241–302, doi:10.1080/09506608.2016.1219481

[23] Q. Zheng, Y. Geng, S. Wang, Z. Li, J. K. Kim, Effects of functional groups on the mechanical and wrinkling properties of graphene sheets, Carbon, 48 (**2010**) 15, 4315–4322, doi:10.1016/j.carbon.2010.07.044

[24] E. Cadelano, P. L. Palla, S. Giordano, L. Colombo, Elastic properties of hydrogenated graphene, Phys. Rev. B, 82 (**2010**), 235414, doi:10.1103/PhysRevB.82.235414

[25] C. J. Xie, M. B. Tong, F. Liu, Z. G. Li, Y. Z. Guo, X. C. Liu, Dynamic tests and constitutive model for 7075-T6 aluminum alloy, Journal of Vibration and Shock, 33 (**2014**) 18, 110–114, doi:10.13465/j.cnki.jvs.2014.18.018

[26] X. Wang, F. Jiang, T. Zhang, L. Wang, Study on dynamic mechanical properties and constitutive model of ¹⁰B/Al composite compared with its matrix of high-purity aluminium, Journal of Materials Science, 55 (**2019**) 2, 748–761, doi:10.1007/s10853-019-03949-z